Article

Photoexcitation and Relaxation Dynamics of Catecholato-Iron(III) Spin-Crossover Complexes

ENACHESCU, Cristian, *et al*.

Abstract

The photophysical properties of the ferric catecholate spin-crossover compounds [(TPA)Fe(R-Cat)]X (TPA=tris(2-pyridylmethyl)amine; X=PF6-, BPh4-; R-Cat=catecholate dianion substituted by R=NO2, Cl, or H) are investigated in the solid state. The catecholate-to-iron(III) charge-transfer bands are sensitive both to the spin state of the metal ion and the charge-transfer interactions associated with the different catecholate substituents. Vibronic progressions are identified in the near-infrared (NIR) absorption of the low-spin species. Evidence for a low-temperature photoexcitation process is provided. The relaxation dynamics between 10 and 100 K indicate a pure tunneling process below 40 K, and a thermally activated region at higher temperatures. The relaxation rate constants in the tunneling regime at low temperature, kHL(T0), vary in the range from 0.58 to 8.84 s-1. These values are in qualitative agreement with the inverse energy-gap law and with structural parameters. A comparison with ferrous spin-crossover complexes shows that the high-spin to low-spin relaxation is generally faster for ferric complexes, owing to the [...]

Reference

ENACHESCU, Cristian, *et al*. Photoexcitation and Relaxation Dynamics of Catecholato-Iron(III) Spin-Crossover Complexes. *ChemPhysChem*, 2006, vol. 7, no. 23, p. 1127-1135

DOI : 10.1002/cphc.200500671

DOI: 10.1002/cphc.200500671

Photoexcitation and Relaxation Dynamics of Catecholato–Iron(III) Spin-Crossover Complexes

Cristian Enachescu,[c] Andreas Hauser,*[a] Jean-Jacques Girerd,[b] and Marie-Laure Boillot*[b]

The photophysical properties of the ferric catecholate spin-crossover compounds [(TPA)Fe(R-Cat)]X (TPA = tris(2-pyridylmethyl)-amine; X = PF_6^-, BPh_4^-; R-Cat = catecholate dianion substituted by R = NO_2, Cl, or H) are investigated in the solid state. The catecholate-to-iron(III) charge-transfer bands are sensitive both to the spin state of the metal ion and the charge-transfer interactions associated with the different catecholate substituents. Vibronic progressions are identified in the near-infrared (NIR) absorption of the low-spin species. Evidence for a low-temperature photoexcitation process is provided. The relaxation dynamics between 10 and 100 K indicate a pure tunneling process below ≈40 K, and a thermally activated region at higher temperatures. The relaxation rate constants in the tunneling regime at low temperature, $k_{HL}(T \rightarrow 0)$, vary in the range from 0.58 to 8.84 s^{-1}. These values are in qualitative agreement with the inverse energy-gap law and with structural parameters. A comparison with ferrous spin-crossover complexes shows that the high-spin to low-spin relaxation is generally faster for ferric complexes, owing to the smaller bond length changes for the latter. However, in the present case the corresponding rate constants are smaller than expected based on the single configurational coordinate model. This is attributed to the combined influence of the electronic configuration and the molecular geometry.

1. Introduction

A thermally-induced $S = 1/2 \leftrightarrow S = 5/2$ spin crossover[1] for an iron(III) catecholate complex was first described for a solid sample of [(TPA)Fe(III)(Cat)]BPh_4 (TPA = tris(2-pyridylmethyl)-amine, Cat = catecholate) by Simaan et al.[2] This complex was considered to be a functional model for catechol dioxygenases.[3] However, in contrast to the $S = 5/2$ high-spin (HS) ground state observed for a number of enzymes[4] as well as for some corresponding functional models,[3] the magnetic behavior of [(TPA)Fe(Cat)]BPh_4 indicates a thermodynamically stable $S = 1/2$ low-spin (LS) state at low temperature and an entropy-driven LS to HS transformation at high temperature. The phenomenon of thermal spin crossover was also observed for a set of close analogues of the above compound, both in the solid state[5,6] as well as in solution.[7] As far as the intradiol cleavage activity is concerned, Que and co-workers[8] and others[9,10] have shown that there is a strong correlation between the reactivity in the presence of dioxygen and the radical character of the catecholate substrate as a ligand. The analysis of the intersite interaction was based on the comparison of the energies of the corresponding ligand-to-metal charge-transfer (LMCT) transitions localized in the NIR–visible range. More recently, evidence for a significant quantum mixing of the Fe(III)Cat and Fe(II)SQ configurations (SQ = semiquinonate monoanion) in both spin states was provided by density functional theory (DFT) calculations.[11] This mesomeric effect accounts for the abnormal spin density on the dioxolene group as well as on the iron ion.

In the series of iron(III) compounds to be studied here, namely [(TPA)Fe(DNC)]PF_6 (**1**), [(TPA)Fe(TCC)]PF_6 (**2**), and [(TPA)Fe(Cat)]BPh_4 (**3**) (DNC = 4,5-dinitrocatecholate, TCC = 3,4,5,6-tetrachlorocatecholate), both the charge-transfer character between the dioxolene and the metal ion site and the spin-crossover characteristics vary. Indeed, for the catecholate substituted with the more electron withdrawing groups (R = NO_2, Cl) a prevailing ferric catecholate configuration of the complex can be expected from their properties in solution (chemical reactivity, UV/Vis spectra) as well as their X-ray single crystal structures.[6] The gradual spin transitions of the solid compounds of **1** and **2** are centered at transition temperatures of 224 and 204 K, respectively. In contrast, the spin transition for **3** takes place in a two-step process centered at 92.5 K.[2]

Herein, we investigate the photoexcitation and relaxation properties of the above set of catecholate iron(III) complexes by laser flash photolysis. The corresponding experiments, essentially carried out on solid samples, serve to probe the characteristics of the excited state in relation to both the spin-

[a] *Prof. A. Hauser*
Département de Chimie Physique, Université de Genève
Bâtiment de Sciences II
30, quai Ernest-Ansermet, 1211 Genève 4 (Switzerland)
Fax: (+41) 22-379-6103
E-mail: andreas.hauser@unige.ch

[b] *Prof. J.-J. Girerd, Dr. M.-L. Boillot*
Equipe de Chimie Inorganique, UMR CNRS 8182, ICMMO, Bât 420
Université Paris-Sud, 91405 Orsay cedex (France)
E-mail: mboillot@icmo.u-psud.fr

[c] *Dr. C. Enachescu*
Faculty of Physics, Department of Solid State and Theoretical Physics
"Alexandru Ioan Cuza" University, Blvd. Carol I, 11, 700506, Iasi (Romania)

crossover behavior and the charge-transfer character within the ground state. The basis of our work is the light-induced spin-crossover process, known by the acronym of LIESST[12] (light-induced excited spin-state trapping). LIESST was initially established at cryogenic temperatures for iron(II) spin-crossover compounds, for which photoexcitation into ligand-field or charge-transfer bands of the LS species results in a quantitative population of the HS state via intersystem-crossing processes. Below the thermal transition temperature, this light-induced HS state is a long-lived metastable state. The relaxation from the HS state back to the LS ground state occurs by a tunneling process, which for some compounds is very slow below 50 K, and which becomes thermally activated above that temperature. In addition to the direct HS→LS relaxation, the LS ground state can also be restored by specific conditions of photoexcitation even at the lowest temperatures (reverse LIESST). Among the different parameters that govern the lifetime of the metastable HS state, the variation of the metal–ligand bond length has a major influence. This feature has been confirmed by the comparison of the relaxation dynamics of iron(II), iron(III),[13,14] and cobalt(II)[15] complexes. The large structural reorganization of the coordination core leads to a significant horizontal displacement of the potential wells and a small overlap of the vibrational wavefunctions of the LS and the HS states. As a consequence, the Franck–Condon factor and therefore the HS→LS relaxation rate constant, k_{HL}, increase exponentially with decreasing bond-length difference, that is, $k_{HL}(Fe(II)) < k_{HL}(Fe(III)) < k_{HL}(Co(II))$. Whereas long-lived metastable HS states are quite common in iron(II) spin-crossover compounds, to date only one such state has been reported for an iron(III) complex exhibiting a strongly cooperative spin-crossover process.[16] In addition, relaxation studies on iron(II) spin-crossover systems are plentiful, while studies on other spin-crossover systems are comparatively scarce, and, with one exception,[13] they are limited to work at ambient temperature and in solution.[14]

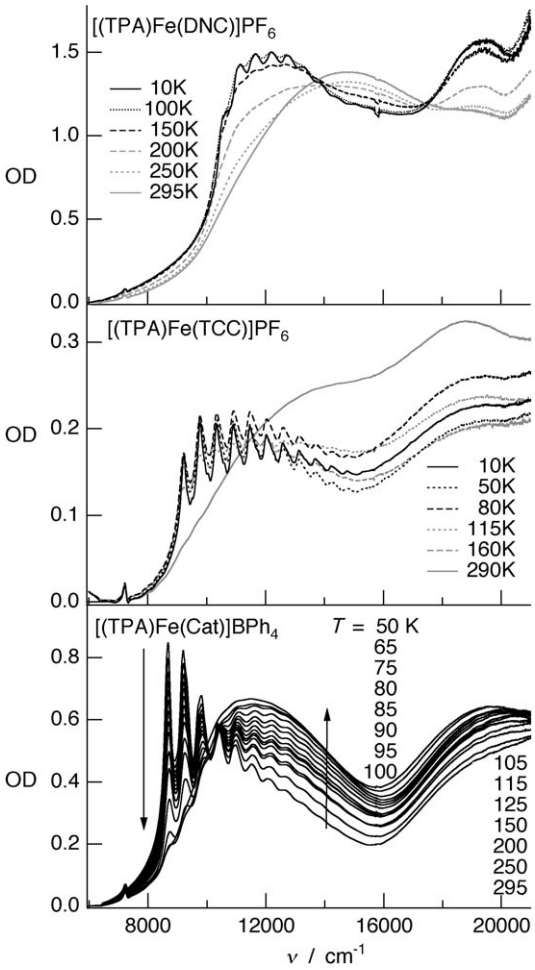

Figure 1. Temperature-dependent absorption spectra (OD = optical density) of microcrystalline powders of **1**, **2**, and **3** dispersed in KBr. Arrows indicate the evolution of the spectra with increasing temperature.

2. Results

2.1. The Thermal Spin Transition

The thermal spin transition from the $S = 1/2$ LS state to the $S = 5/2$ HS state of compound **1** has been followed both by magnetic susceptibility measurements as well as Mössbauer spectroscopy.[11] All data are in agreement with a metal-centered spin transition and show no indication of a thermally accessible catecholate→iron(III) charge-transfer state, as is often observed in analogous cobalt(III) catecholate complexes.[17] Figure 1 presents the absorption spectra of **1**, **2**, and **3** and their thermal evolution between 10 and 300 K. These spectra show strong similarities. In agreement with the magnetic and the Mössbauer data, and as previously analyzed for **3**,[11] they characterize the spin-crossover process and the LMCT transitions[18] in both spin states. As the LS→HS transformation takes place, the intensities of the structured absorption bands of the LS species localized in the NIR range decrease, and new absorption bands assigned to the HS species clearly appear in the visible range. The same characteristic behavior has been reported for other iron(III) spin-crossover complexes having $[N_4O_2]$ coordination.[13] The key difference of the present series of complexes is that the catecholate ligand is easier to oxidize than the ligands in these complexes, and therefore the optical LMCT transition, corresponding to a vertical catecholate→iron(III) charge-transfer, is shifted to substantially lower energy. In fact, the LMCT transitions are significantly modulated according to the nature of the catecholato substituent, which is consistent with the different colors of the solids observed at room temperature (**1** is dark green; **2** and **3** are dark violet). The low-energy transitions (denoted CT1 in Table 1), both in the LS and the HS state, are red-shifted by approximately 3300 cm^{-1} when the electron-donating character of the catecholate substituent increases in the series $R = NO_2$ (**1**) < Cl (**2**) < H (**3**). As expected, the tendency shown by these data, together with the one characterized for solutions,[6] is a decrease of the charge-transfer energy with the electron-donating character of the catecholate group. This is also consistent with different correlations reported by Funabiki and co-workers and others.[5,19] The vibronic progression of approximately 550 cm^{-1}, which appears as a fingerprint of the LS charge-transfer absorption, was previ-

Table 1. Spectroscopic data for compounds **1**, **2**, and **3** dispersed in KBr, LMCT transition denoted CT.

Compound	Label	CT1(LS) [cm^{-1}]	CT2(LS) [cm^{-1}]	CT1(HS) [cm^{-1}]	CT2(HS) [cm^{-1}]	ν_0(LS) [cm^{-1}]
[(TPA)Fe(DNC)]PF6	**1**	11800	19450	14810	19010[a]	530
[(TPA)Fe(TCC)]PF6	**2**	10200	19510	13380	18830	560
[(TPA)Fe(Cat)]BPh4	**3**	8900	>20000	11490	19720	520–560

[a] Unresolved band.

ously assigned to the FeO_2C_2 chelate ring mode.[11] The frequency deduced from the spacing between two successive components of the progression slightly varies for the studied complexes as $\nu_0(\mathbf{1}) < \nu_0(\mathbf{3}) < \nu_0(\mathbf{2})$. The well-resolved progression of the catecholate→iron(III) charge-transfer band of the LS species indicates that the geometry of the charge-transfer state is similar to the one of the ground state. In fact, the first member of the progression directly gives the zero-point energy difference between the two states. The vertical energy difference between the iron(III) HS state and the corresponding LMCT state is at still higher energy. The absorption band associated with this transition is unstructured and much broader. This is due to the larger bond-length difference between the iron(III) HS state and the iron(II) HS charge-transfer state. But even taking this into account, the zero-point energy of the iron(II) HS charge-transfer state is still much too high in energy to be populated thermally, that is, it must be of the order of 10000 cm^{-1}.

2.2. Photoexcitation in Spin-Crossover Catecholate Systems

Figure 2a shows the evolution of the spectra recorded for **3** between 10 and 50 K in the NIR, that is, in the spectral region in which the evolution is most easily discernible. In fact, the apparent trend observed in this temperature range is opposite to the one above 50 K shown in Figure 1. Whereas the intensity of the lowest energy band at 8900 cm^{-1} with the prominent vibrational structure decreases at the expense of the HS charge-transfer bands centered at 11490 and 19720 cm^{-1} with increasing temperature above 50 K, the opposite behavior is observed between 10 and 50 K. The low-temperature spectra in the NIR indicate a partial depopulation of the LS state. This partial depopulation is due to the permanent broadband illumination with the W–halogen lamp of the Fourier transform infrared (FTIR) spectrometer. This can be verified by changing the irradiation conditions. As shown in Figure 2b, the bleaching observed in the 10 K spectrum can be partly reversed when a grey filter (2%) or an IR filter is put into the light beam of the spectrometer. In contrast, the use of a visible filter results in the previous 10 K spectrum. Thus, below 50 K, a partial steady-state population of a metastable state occurs when the sample is excited continuously in the NIR, that is, into the lowest energy LMCT band of the LS species. The key question to answer regards the nature of the light-induced state. In analogous cobalt(III) catecholate complexes, the thermal equilibrium and the light-induced population of a metastable state was shown to occur between the cobalt(III) catecholate LS ground state and the thermally accessible cobalt(II) semiquinonate HS charge-transfer state. As discussed above, for the iron(III) catecholate complexes considered here, the charge-transfer state is at comparatively high energy and is thus not expected to have a sufficiently long life-

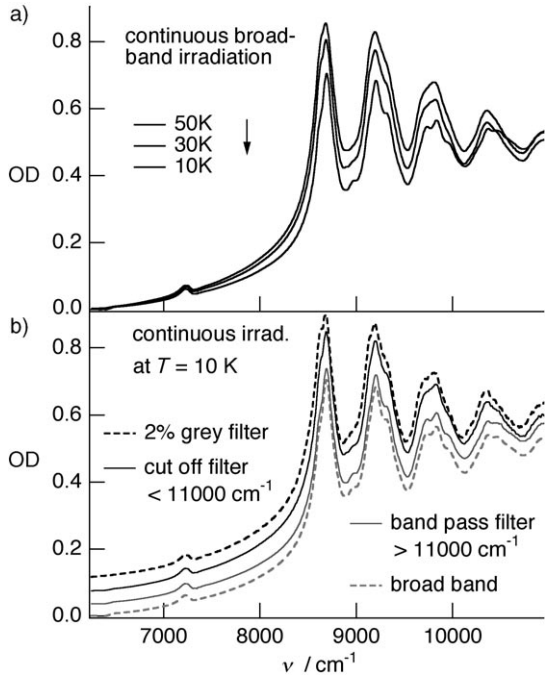

Figure 2. Absorption spectra of **3** in the NIR region under continuous irradiation from a W–halogen lamp: a) broadband as function of temperature between 10 and 50 K. b) at 10 K under broadband irradiation full intensity (100%) and reduced intensity (2%), in the NIR ($\nu_{ir} < 11000\ cm^{-1}$) and in the visible ($\nu_{ir} > 11000\ cm^{-1}$) using spectral filters.

time for the above steady-state population. Rather, the initially excited charge-transfer state is very short lived and the system relaxes rapidly to the low-lying iron(III) HS state, as has been observed for a number of iron(III) spin-crossover complexes in the solid state and in solution.[13,14] It would of course be useful to have an independent proof of the nature of the light-induced state. However, with a lifetime of less than one second, and a rather low quantum efficiency, Mössbauer spectroscopy and classical magnetic susceptibility measurements on the metastable state are not feasible.

2.3. The High-Spin→Low-Spin Relaxation

The photoexcitation of the iron(III)-catecholato complex **3** at low temperatures being established, the relaxation properties of the photoexcited states were thoroughly investigated for compounds **1** to **3** using a pulsed Nd:YAG laser. For complex **3**, the best available photoexcitation wavelength was found to be equal to the fundamental wavelength of the Nd:YAG laser at 1064 nm (9400 cm^{-1}), that is close to the maximum of the

LMCT band of the LS species, and the relaxation process was monitored by the transient absorption of the LMCT band of the HS species at 750 nm (13 300 cm^{-1}), as described in the Experimental Section. The metastable state is formed from the initially excited high-energy LMCT state within the pulse width of the laser of 7 ns. The positive transient absorption at this wavelength is strong evidence for the iron(III) HS state as the metastable state, and it virtually excludes a HS iron(II) charge-transfer state, as iron(II) complexes in the HS state usually only absorb very weakly in the visible. Figure 3 shows the observed

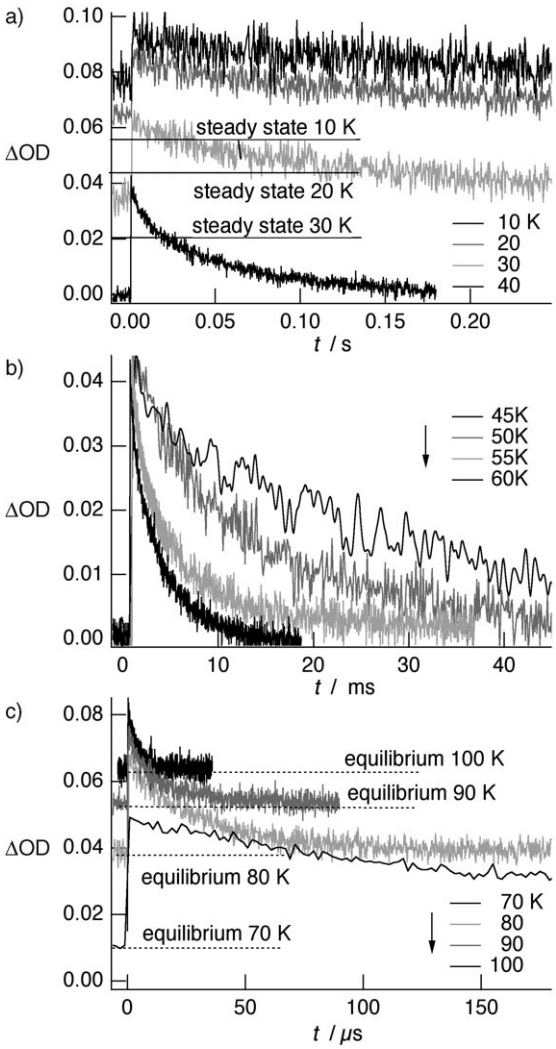

Figure 3. HS→LS relaxation curves for compound **3** following pulsed laser excitation at 1064 nm. a) Below 40 K, where the relaxation is in competition with the additional excitation from the continuous probe beam, b) in the interval 40 K < T < 70 K, where the relaxation is complete, and c) above 70 K, where the thermal spin-transition sets in.

decay curves recorded at temperature between 10 and 100 K. The decay curves can be satisfactorily fitted with a single exponential curve. However, the extraction of the correct HS→LS relaxation rate constants, k_{HL}, from the observed rate constants, k_{obs}, should take into account a number of different features: the relaxation curves were actually measured under the permanent irradiation from the 50 W W–halogen source. Below 40 K, this results in the steady-state population of the HS state described above in addition to the transient population due to the pulsed excitation. Above 70 K, the thermal population likewise results in a steady-state population of the HS state in addition to the transient population. In both cases, the relaxation curves do not return to zero HS population and k_{obs} is larger than k_{HL}. The observed rate constant is given by Equation (1):

$$k_{HL} = k_{obs}(1-\gamma_{HS\ SS}) \quad (1)$$

where $\gamma_{HS\ SS}$ is equal to the steady-state HS fraction, either due to the continuous irradiation or due to the thermal population (see Experimental Section). In the interval 40 K < T < 70 K, the above effects become negligible. Figure 4a shows both k_{obs} as

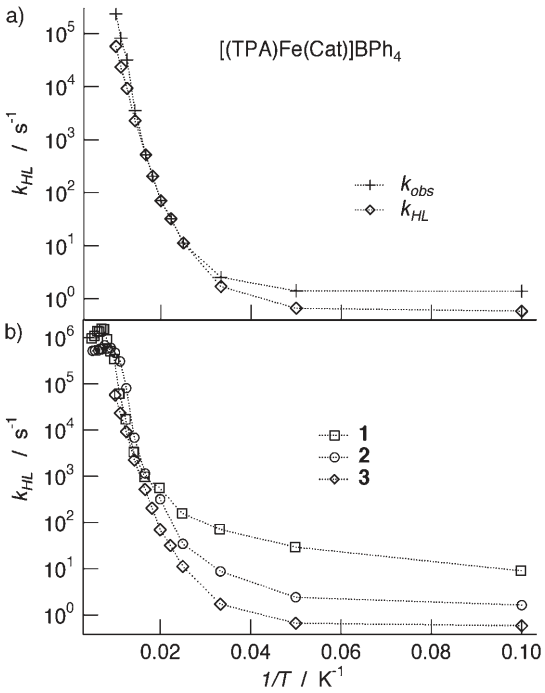

Figure 4. a) Observed decay rate constant k_{obs} and HS→LS relaxation rate constant k_{HL} plotted on logarithmic scale versus 1/*T* for compound **3**. b) HS→LS relaxation rate constants plotted as ln(k_{HL}) versus 1/*T* for compounds **1**, **2**, and **3**.

well as k_{HL} for compound **3**. From 10 to 100 K, the relaxation process is accelerated by five-orders of magnitude, with $k_{HL}(10\ K) = 0.58\ s^{-1}$ ($\tau = 1.7$ s) and $k_{HL}(100\ K) = 57\,400\ s^{-1}$ ($\tau = 17\ \mu s$). The actual temperature dependence follows the predictions for a nonadiabatic multiphonon relaxation process in the strong coupling limit according to Buhks et al.,[20] with temperature-independent tunneling below ≈40 K and the expected thermally activated regime in the high-temperature range. The effective activation energy is estimated to be $E_a \approx 540(25)\ cm^{-1}$.

Analogous experiments were performed for the other two catecholato–iron(III) complexes. For **2**, the excitation wavelength was likewise chosen at 1064 nm and the relaxation was monitored at 555 nm (18 000 cm^{-1}). The former is on the low-

energy rise of the LMCT transition of the LS species, the latter corresponds to the maximum of the LMCT absorption band of the HS species. For compound **1**, the excitation and monitoring were effected at 532 nm (18800 cm^{-1}) and 510 nm (19600 cm^{-1}), respectively. Both wavelengths correspond to a higher-energy transition of the LS species. For **2**, the monitoring at 555 nm shows a transient absorption, whereas **1** exhibits transient bleaching at 510 nm. In fact, this constitutes further evidence for a rapid population of the low-lying HS state as a result of the excitation into higher energy transitions, which in turn is followed by the simple HS→LS relaxation. Figure 5

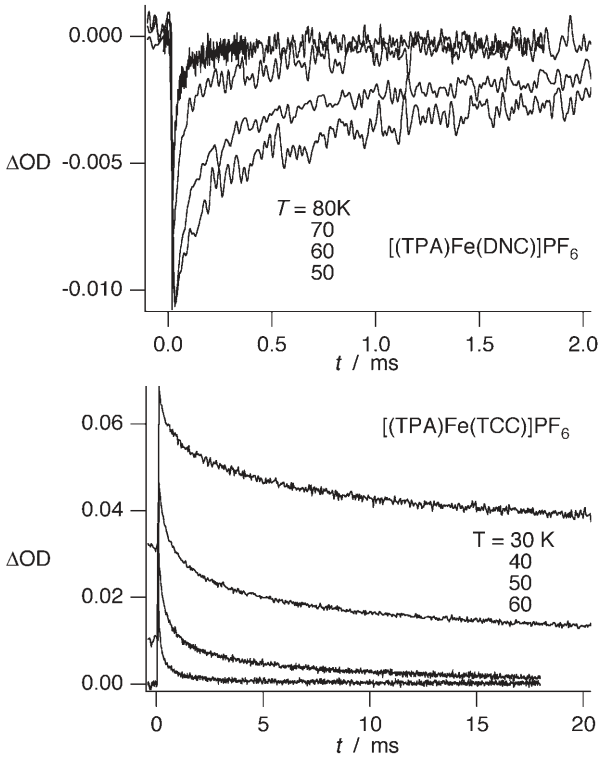

Figure 5. Representative HS→LS relaxation curves at selected temperatures for compounds **1** (top) and **2** (bottom) dispersed in KBr.

shows representative relaxation curves for both compounds. As observed for **3**, the steady-state limit below 40 K increases when the temperature decreases, because of the continuous photoexcitation from the W–halogen lamp of the probe beam. For both **1** and **2**, the relaxation curves deviate substantially from single-exponential behavior. The average relaxation rate constants were therefore evaluated as described in the Experimental Section. They are shown together with k_{HL} for **3** on a logarithmic scale versus $1/T$ in Figure 4b. As expected, the temperature behavior for all three compounds is characteristic for low-temperature tunneling below ≈50 K and a thermally activated process at higher temperature. The corresponding low-temperature rate constants and the activation parameters are collected in Table 2. With values of 0.58, 1.83, and 8.84 s^{-1}, the low-temperature tunneling rate-constant increases by an order of magnitude in the series **3**, **2**, **1**. The activation parameters are, within experimental accuracy, identical. At this stage, a comment on the apparent slowing down of the HS→LS relaxation for compounds **1** and **2** above 130 K is in order. This slowing down is not real, but it is due to a thermal effect. The samples suffer a small temperature jump under the effect of the laser pulse. Below the thermal spin-transition, this has a negligible effect on the relaxation curves. However, within the transition curve, in particular if it is comparatively steep, this gives rise to an additional increase of the HS fraction. If the thermalization of the sample occurs over a larger time interval than the relaxation itself, the apparent relaxation curve is characterized by the thermalization rather than the relaxation.

3. Discussion

The above data on the HS→LS relaxation in iron(III) catecholate complexes can be further analyzed and compared to the results for other iron(III) as well as iron(II) spin-crossover systems. The basis of such an analysis is the theory of nonadiabatic multiphonon relaxation.[20] In the case of strong vibronic coupling, that is for a comparatively small driving force (small energy difference between the initial and final states) and large geometrical rearrangements (large metal–ligand bond length difference between the two states), this theory predicts a pure tunneling process through the barrier between the potential wells of the two states at low temperatures, and a thermally activated process to be regarded as tunneling from thermally excited vibrational levels of the initial state at elevated temperatures. The low-temperature tunneling rate-constant is given by Equation (2):

Table 2. The transition temperature $T_{1/2}$,[2,6] the mean difference in metal–ligand bond lengths between the HS and the LS state Δr_{HL},[6,11] bond lengths and bond angles of the HS species, the low-temperature tunneling rate constant k_{HL} ($T\rightarrow 0$), and activation parameters A and E_a for compounds **1**, **2**, and **3** dispersed in KBr.

	$T_{1/2}$ [K]	Δr_{HL}[a] [Å]	Bond lengths [Å]	Bond angles [°]	A [s^{-1}]	E_a [cm^{-1}]	$k_{HL}(T\rightarrow 0)$ [s^{-1}]
[(TPA)Fe(DNC)]PF_6	224	0.12	1.90–2.15	76.6–103.1 155.0–175.7	10^9	565(50)	8.84
[(TPA)Fe(TCC)]PF_6	204	0.16	1.87–2.13	77.1–104.1 155.6–175.3	10^9	520(40)	1.63
[(TPA)Fe(Cat)]BPh_4	92.5	0.16	1.89–2.16[b]	76.0–104.3[b] 154.5–173.6[b]	10^8	540(25)	0.58

[a] Values of Δr_{HL} are extrapolated for a complete spin-crossover process. [b] Refers to the crystalline site exhibiting a high-temperature spin crossover.

$$k_{HL}(T \rightarrow 0) = \frac{2\pi}{\hbar^2\omega}\beta_{HL}^2|\langle\chi_n \mid \chi_0\rangle|^2 \quad (2)$$

where β_{HL} is the electronic matrix element coupling of the two states and can be calculated by higher-order spin–orbit coupling,[20] ω is the vibrational frequency of the accepting mode, and Equation (3) is the Franck–Condon factor for the overlap between the $m=0$ vibrational wavefunction of the HS state and the $m'=n$ vibrational wavefunction of the LS state:

$$|\langle\chi_n \mid \chi_0\rangle|^2 = \frac{e^{-S}S^n}{n!} \quad (3)$$

In order to ensure energy conservation, $m'=m+n$, where the reduced energy gap, Equation (4):

$$n = \frac{\Delta E_{HL}^0}{\hbar\omega} \quad (4)$$

expresses the zero-point energy difference between the two states, ΔE_{HL}^0, and the Huang–Rhys factor, Equation (5):

$$S = \frac{1/2 f \Delta Q_{HL}^2}{\hbar\omega} \quad (5)$$

expresses the reorganization energy in units of $\hbar\omega$. The key parameters for the tunneling rate constant are thus ΔE_{HL}^0 and ΔQ_{HL}. ΔE_{HL}^0 is directly related to the thermal transition temperature $T_{1/2}$, ΔQ_{HL} is basically given by the bond-length difference between the two states, that is, in terms of the totally symmetric breathing mode $\Delta Q_{HL}=\sqrt{6}\Delta r_{HL}$. In addition to $k_{HL}(T\rightarrow 0)$, Table 2 reports the transition temperatures $T_{1/2}$ and the variation of the mean metal–donor-atom bond-length, bond lengths, and bond angles for the HS species, estimated from the magnetic measurements and the crystalline structures reported in refs. [6, 11], respectively.

For compounds **1** and **2**, the transition temperatures, and hence the vertical shift of the potential wells, are comparable. The fact that $k_{HL}(T\rightarrow 0)$ is larger for **1** than for **2** has therefore to be attributed to the geometric factor. Indeed, according to Table 2 $\Delta r_{HL}(\mathbf{1}) < \Delta r_{HL}(\mathbf{2})$, therefore the Huang–Rhys factor for **1** is smaller, and the relaxation rate constant larger, than for **2**. On the other hand, the values of Δr_{HL} for **2** and **3** are almost equal, but the transition temperature is higher for **2**. This results in a smaller reduced energy gap and therefore a smaller relaxation rate constant for **3** as compared to **2**. Qualitatively, the ordering of the relaxation rate constants is thus in agreement with the inverse energy-gap law and the structural parameters.

The above results show that both the structural and energetic parameters vary in the series of catecholate complexes. The question is, how is the ground-state mixture of Fe(III)Cat and Fe(II)SQ configurations, as borne out by the DFT calculations, related to this observation. The charge-transfer character is partly reflected in the value of Δr_{HL}: the larger the contribution from the ferrous configuration, the larger Δr_{HL}. Complex **1** with the most electron withdrawing group on the catecholate moiety, and thus the smallest charge-transfer contribution, has the smallest value of Δr_{HL}. In addition, for **1**, the lowest energy LMCT transitions are found in the visible range. This indicates a weaker interaction between the frontier orbitals of the ligand and the iron center, in agreement with the weaker donor character of 4,5-dinitrocatecholato in comparison with the catecholato ligand of **3**, for which the corresponding LMCT band is found in the NIR.[11] These different observations suggests a combined effect of the usual parameters involved in the nonadiabatic multiphonon relaxation and the charge-transfer interaction between the metal ion and the dioxolene ligand.

How do the above values of $k_{HL}(T\rightarrow 0)$ compare to literature values on other iron(III) spin-crossover systems, and how do they compare to the extremely slow relaxation observed for iron(II) spin-crossover systems at low temperatures? Table 3 collects the thermal transition temperatures $T_{1/2}$, the mean bond length differences Δr_{HL}, the variation range of bond lengths and bond angles for the HS species, the low-temperature tunneling rate constants $k_{HL}(T\rightarrow 0)$, and the energies of the lowest LMCT transitions of both the HS and the LS species from previously reported ferric spin-crossover complexes incorporating Schiff base ligands $[Fe(acpa)_2]PF_6$, $[Fe(bzpa)_2]PF_6$ and $[Fe(Sal_2tr)]PF_6$ (Hacpa = *N*-(1-acetyl-2-propylidene)-2-pyridylmethylamine; Hbzpa = *N*-(1-benzoyl-2-propylidene)-2-pyridylmethylamine and H_2Sal_2tr = bis(salicylalimino)triethylenetetramine).[13] These iron(III) Schiff base complexes possess a $[FeN_4O_2]$ coordination core[21] similar to the one of the systems studied here, except that the Δr_{HL} values and the distortions of the coordination polyhedron (see Tables 2 and 3) are smaller.[6, 11, 20] This latter observation is due to the chelation of the TPA ligand via five-membered and interconnected chelate

Table 3. Thermal transition temperatures $T_{1/2}$, mean bond-length differences Δr_{HL}, bond lengths, and bond angles refer to the HS species; the low-temperature tunneling rate constant $k_{HL}(T\rightarrow 0)$, and the energies of the lowest LMCT transitions of both the HS and the LS species.

	$T_{1/2}$ [K]	Δr_{HL} [Å]	Bond lengths [Å]	Bond angles [°]	$k_{HL}(T\rightarrow 0)$ [s^{-1}]	$CT1^{LS}$ [cm^{-1}]	$CT1^{HS}$ [cm^{-1}]	
$[Fe(Sal_2tr)]PF_6$	250	unknown			10^2	16100	20450	P/Bn
$[Fe(Sal_2tr)]PF_6$	130				3.9×10^2	15650	19550	KBr
$[Fe(acpa)_2]PF_6$	225	0.13[b]	1.94–2.15[a]	77.5–97.1[a] 166.0–171.1[a]	1.8×10^4	14680	18100	P/Bn
$[Fe(acpa)_2]PF_6$	190				1.9×10^2	14050	16660	KBr
$[Fe(bzpa)_2]PF_6$	240	unknown			5.1×10^4	14180	17500	P/Bn
$[Fe(bzpa)_2]PF_6$	220				3.3×10^2	13810	17060	KBr
$[Fe(pap)_2]PF_6$	150[a]	unknown			$\approx10^{-3}$[b]	10500[b]	13500[b]	KBr

All data from ref. [13], except for [a] which is from ref. [21], and [b] which is from ref. [22].

rings. The relaxation rates in the tunneling regime at low temperature $k_{HL}(T\rightarrow 0)$ vary in the range 10^2–$5\times10^4\ s^{-1}$. These values are two to three orders of magnitude larger than those obtained herein. This tendency is especially clear for **1**, whose characteristics are closer to a ferric complex, and the Δr_{HL} and $T_{1/2}$ parameters are comparable to those of the above Schiff base complexes. Note that replacing an electron-donating catecholate group by a Schiff base phenolate group provokes a shift of the LMCT bands towards high energy, and a boost of the relaxation rates. As mentioned above, this observation suggests that the more efficient the mechanism of electronic delocalization (as found for Fe(III) catecholate), the slower the relaxation rates in the tunneling regime. In addition, Table 3 includes preliminary results[22] on the (to-date) only iron(III) spin-crossover compound with a truly long-lived metastable HS state at low temperature, namely $[Fe(pap)_2](PF_6)\cdot MeOH$ (Hpap = 2-hydroxyphenyl-(2-pyridyl)-methaneimine).[16] For this compound, $k_{HL}(T\rightarrow 0)\approx 10^{-3}\ s^{-1}$, that is, two to three orders of magnitude smaller than for the series of catecholate complexes. In the absence of any structural information, this latter fact has been attributed to strong cooperative effects.[16]

Figure 6 shows $k_{HL}(T\rightarrow 0)$ as a function of $T_{1/2}$ for all iron(III) spin-crossover complexes of Tables 2 and 3, and for comparison for a series of iron(II) complexes from the literature.[12] Whereas for the series of iron(II) systems, $k_{HL}(T\rightarrow 0)$ as a function of $T_{1/2}$ falls within the comparatively narrow band calculated for a value of the Huang–Rhys factor $S = 45\pm5$ estimated from the average value of $\Delta r_{HL}\approx 0.2$ Å[23] for iron(II) spin-crossover systems,[12] the behavior of the iron(III) systems is much more erratic. Except for the systems with the "innocent" Schiff base ligands, the HS→LS relaxation is slower than expected based on the simple single configurational coordinate model with an estimated value of $S = 25\pm5$. In addition to the electronic effects discussed above, this suggests that the asymmetry of the $[FeN_4O_2]$ unit, in particular the chelation of the catecholate-TPA, and the associated route with distortions along a more complex configurational coordinate play an important role. It may be noted that some notable exceptions for iron(II) systems, namely the astonishingly long lifetime of the light-induced HS state in the classic LS complex $[Fe(terpy)_3]^{2+}$ (terpy = 2,2′-6,2″terpyridine) has likewise been attributed to the asymmetric coordination and the breakdown of the single configurational coordinate model.[24,25]

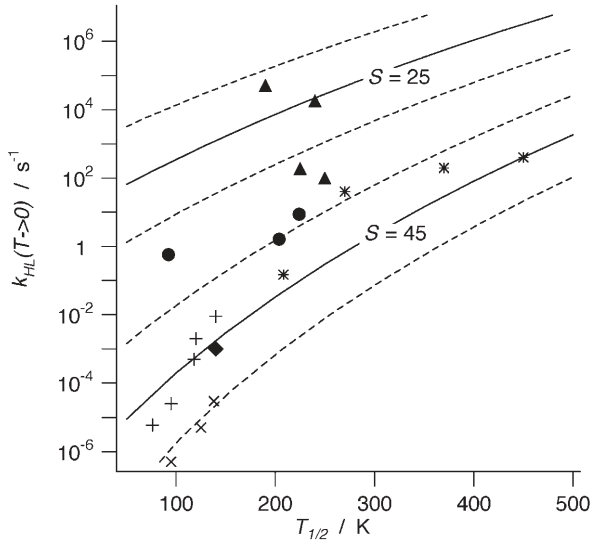

Figure 6. The low-temperature tunneling rate constants for iron(III) and iron(II) spin-crossover compounds. Iron(II): (▲) the acpa, bzpa, and saltrien complexes,[13,20] (●) the catecholates, (◆) the pap complex.[16] Iron(II):[12] (*) the mepy-tren family, (+) the picolylamine complexes, and (×) the tetrazole complexes. —— and -----: predicted according to the theory of multiphonon relaxation with $S = 45\pm5$ for iron(II) and $S = 25\pm5$ for iron(III).

4. Conclusions

This investigation on a series of catecholato–iron complexes in the solid state has shown the occurrence of a photoexcitation process leading to a LS→HS conversion at low temperatures. The rate constants for the subsequent HS→LS relaxation were determined over a range of temperatures, from the tunneling to the thermally activated regime. A comparison with previously reported values for iron(II) and iron(III) spin-crossover compounds reveals a more complex behavior for the latter. The lifetimes of the HS photoexcited states of ferric spin-crossover complexes span a broader range than the one expected from the application of the single configurational coordinate model. Different features are proposed to account for this interesting observation: In addition to the structural characteristics, comparatively small variations of the metal–ligand bond lengths, and large distortions of the asymmetric coordination core, the catecholato–iron systems also show an increase in the lifetime of the HS photoexcited state with the charge-transfer interaction between the metal ion and the dioxolene ligand. This is consistent with a combined effect of the electronic and the geometric structures for iron(III) compounds with noninnocent ligands. However, a quantitative discussion of the role of a more complex reaction coordinate for the HS→LS relaxation in iron(III) systems requires a more extended structural data base than is currently available.

Experimental Section

Preparation of Samples: The above-mentioned series of compounds in the form of microcrystalline powders was prepared according to literature procedures.[2,6,11] For optical measurements, small amounts of the microcrystalline solids were dispersed in KBr pellets. It was checked that the spectral and the spin-crossover characteristics of the compounds were not significantly changed by this treatment.[11]

Absorption Spectra: Variable-temperature NIR/Vis spectra were recorded from 6000 to 22000 cm^{-1} using an IFS66/S Bruker FTIR spectrometer. The light source was provided by a 50 W tungsten–halogen lamp and the signal was measured using either a Si (9000–22000 cm^{-1}) or a Ge (6000–12000 cm^{-1}) detector. Temperatures down to 11 K were achieved in a closed-cycle helium cryostat (Oxford Instruments CCC1204). Note: in the FT spectrometer, the

polychromatic light from the W–halogen lamp continuously irradiates the sample.

Photoexcitation: Variable-temperature photoexcitation experiments were performed with a pulsed Nd:YAG pulsed laser with a repetition rate from 2 to 20 Hz at $\nu_{exc}=9398\ cm^{-1}$ (1064 nm) for **3** and **2**, and at 18797 cm^{-1} (532 nm) for **1**. For **2** and **3** this corresponds to the lowest-energy LMCT transition of the LS species, for **1** to a higher-energy transition of the LS species. Laser pulses were typically 200 $\mu J\,mm^{-2}$. The relaxation curves were monitored at different probe wavelengths $\nu_{probe}=13333\ cm^{-1}$ (750 nm) for **3**, 18018 cm^{-1} (555 nm) for **2**, and 19608 cm^{-1} (510 nm) for **1**, provided by a 50 W W–halogen lamp. For **2** and **3** this corresponds to the absorption maximum of the LMCT band of the light-induced HS species, for **1** it corresponds to the higher-energy LMCT transition of the LS species. After crossing the sample, the probe beam was dispersed in an 1/4 m double monochromator, then detected with a photomultiplier (Hamamatsu R928) in conjunction with a fast preamplifier. Transient curves were recorded using a digital oscilloscope (Tektronix TDS540B).

Data Evaluation: In order to extract the correct relaxation rate constant in the case of a significant continuous excitation from the probe beam, the following procedure was applied. In the absence of the excitation from the pulsed laser, a photostationary state is quickly established, for which the relaxation and photoexcitation terms are equal. The master equation is given by Equation (6):

$$\frac{d\gamma_{HS}}{dt} = I\sigma(1-\gamma_{HS}) - k_{HL}\gamma_{HS} \tag{6}$$

where γ_{HS} is the HS fraction, and $I\sigma$ and k_{HL} are the photoexcitation and the HS→LS relaxation rate constants, respectively. In the steady state, we have Equation (7):

$$\frac{d\gamma_{HS\_SS}}{dt} = 0 \tag{7}$$

and therefore Equation (8):

$$I\sigma(1-\gamma_{HS\_SS}) = k_{HL}\gamma_{HS\_SS} \tag{8}$$

where $\gamma_{HS\ SS}$ is the HS fraction in the steady state. The observed HS→LS relaxation rate constant, k_{obs}, is determined from Equation (9):

$$\frac{d\gamma_{HS}}{dt} = -k_{obs}\gamma_{HS} \tag{9}$$

Equation (10) follows from a comparison of Equations (6) and (9):

$$k_{obs} = k_{HL} + I\sigma \tag{10}$$

Replacing $I\sigma$ by its value in Equation (8), the relaxation rate constant can be easily calculated by Equation (11):

$$k_{HL} = k_{obs}(1-\gamma_{HS\_SS}) \tag{11}$$

which is equal to Equation (1). The same argument is valid at higher temperatures, where the HS state becomes thermally populated. In that case, the relaxation rate constant for the thermally induced LS→HS conversion, k_{LH}, replaces the photoexcitation term and the final result remains the same. The corresponding values of $\gamma_{HS\ SS}$ can be estimated from the steady-state spectra.

For spin-crossover systems dispersed in KBr, relaxation curves often deviate from single-exponential due to inhomogeneous distributions of the zero-point energy difference and cooperative effects. The average relaxation rate constant of the light-induced state is given by Equation (12):

$$k_{HL} \approx \frac{\int_{t=0}^{t=t_{max}} (\gamma_{HS}(t)-\gamma_{HS\_SS})dt}{\int_{t=0}^{t=t_{max}} t\,(\gamma_{HS}(t)-\gamma_{HS\_SS})dt} \tag{12}$$

In principle, the numerical evaluation according to Equation (12) is straightforward, but in some cases it is impractical, for instance when the distribution is large and the return to the steady-state value $\gamma_{HS\ SS}$ is slow. Alternatively, the quasi-continuous distribution can be approximated as a sum of two monoexponential functions as shown in Equation (13):

$$\gamma_{HS} = A_0 + A_1\cdot\exp(-k_1\cdot t) + A_2\cdot\exp(-k_2\cdot t) \tag{13}$$

Usually, there are no excitation effects of the probe beam, and A_0 is equal to 0; otherwise A_0 takes the value corresponding to the steady state. The average lifetime for the excited state can be written by Equation (14):

$$\tau = \frac{\tau_1\cdot A_1 + \tau_2\cdot A_2}{A_1 + A_2} \tag{14}$$

where $\tau_1=1/k_1$ and $\tau_2=1/k_2$ are the lifetimes of the two considered species. The average relaxation rate constant is then given by Equation (15):

$$k_{HL} = \frac{k_1\cdot k_2\cdot(A_1+A_2)}{k_1\cdot A_2 + k_2\cdot A_1} \tag{15}$$

In the cases where evaluation of the average value of k_{obs} both according to Equation (12) as well as following the approximate double-exponential procedure was possible, there was no significant difference in the resulting value. Thus the two procedures may be considered robust.

Acknowledgements

Financial support from the Swiss National Science Foundation and the MAGMANet NoE of the European Union (Contract: NMP3-CT-2005-515767-2) is gratefully acknowledged. MLB thanks the University of Geneva for providing financial support for this collaboration and J. Sainton for help with the synthesis.

Keywords: charge transfer · iron · laser spectroscopy · photophysics · spin crossover

[1] *Spin Crossover in Transition Metal Compounds, Vols. I–III, Topics in Current Chemistry*, (Eds.: P. Gütlich, H. A. Goodwin) Springer, Heidelberg, **2004**, pp.233 – 235.
[2] A. J. Simaan, M.-L. Boillot, E. Rivière, A. Boussac, J.-J. Girerd, *Angew. Chem.* **2000**, *112*, 202; *Angew. Chem. Int. Ed.* **2000**, *39*, 196.
[3] a) L. Que, Jr., *Bioinorganic Catalysis, 2nd ed.* (Eds.: J. Reedijk, E. Bouwman), Marcel Dekker, New York, **1999**, p. 269; b) L. Que, Jr., M. F. Reynolds in *Metal Ions in Biological Systems, Vol. 37* (Eds.: A. Sigel, H. Sigel), Marcel Dekker, New York, Basel, **2000**, p. 505.
[4] J. D. Lipscomb, A. M. Orville in *Metal Ions in Biological Systems, Vol. 28* (Eds: A. Sigel, H. Sigel), Marcel Dekker, New York, Basel, **1992**, p. 243.
[5] T. Funabiki, A. Fukui, Y. Hitomi, M. Higuchi, T. Yamamoto, T. Tanaka, F. Tani, Y. Naruta, *J. Inorg. Biochem.* **2002**, *91*, 151.
[6] S. Floquet, A. J. Simaan, E. Rivière, M. Nierlich, P. Thuéry, J. Ensling, P. Gütlich, J.-J. Girerd, M.-L. Boillot, *Dalton Trans.* **2005**, 1734.

[7] a) Y. Hitomi, M. Higuchi, H. Minami, T. Tanaka, T. Funabiki, *Chem. Commun.* **2005**, *13*, 1758; b) M. Higuchi, Y. Hitomi, H. Minami, T. Tanaka, T. Funabiki, *Inorg. Chem.* **2005**, *44*, 8810.
[8] a) D. D. Cox, L. Que, Jr., *J. Am. Chem. Soc.* **1988**, *110*, 8085; b) H. G. Jang, D. D. Cox, L. Que, Jr., *J. Am. Chem. Soc.* **1991**, *113*, 9200.
[9] T. Funabiki, A. Mizoguchi, T. Sugimoto, S. Tada, M. Tsuji, H. Sakamoto, S. Yoshida, *J. Am. Chem. Soc.* **1986**, *108*, 2921.
[10] A. Dei, D. Gatteschi, L. Pardi, *Inorg. Chem.* **1993**, *32*, 1389.
[11] A. J. Simaan, M.-L. Boillot, R. Carrasco, J. Cano, J.-J. Girerd, T. A. Mattioli, J. Ensling, H. Spiering, P. Gütlich, *Chem. Eur. J.* **2005**, *11*, 1779.
[12] a) A. Hauser in *Spin Crossover in Transition Metal Compounds, Vol. II, Topics in Current Chemistry 234*, Springer, Heidelberg, **2004**, p. 155; b) S. Decurtins, P. Gütlich, K. M. Hasselbach, H. Spiering, A. Hauser, *Inorg. Chem.* **1985**, *24*, 2174.
[13] a) S. Schenker, A. Hauser, *J. Am. Chem. Soc.* **1994**, *116*, 5497; b) S. Schenker, A. Hauser, R. M. Dyson, *Inorg. Chem.* **1996**, *35*, 4676.
[14] a) I. Lawthers, J. J. McGarvey, *J. Am. Chem. Soc.* **1984**, *106*, 4280; b) J. K. Beattie, *Adv. Inorg. Chem.* **1988**, *32*, 1.
[15] I. Krivokapic, C. Enachescu, M. Zerara, A. Hauser, unpublished results.
[16] a) S. Hayami, Z.-Z. Gu, M. Shiro, Y. Einaga, A. Fujishima, O. Sato, *J. Am. Chem. Soc.* **2000**, *122*, 7126; b) G. Juhász, S. Hayami, O. Sato, Y. Maeda, *Chem. Phys. Lett.* **2002**, *364*, 164.
[17] D. N. Hendrickson, C. G. Pierpont in *Spin Crossover in Transition Metal Compounds, Vol. II, Topics in Current Chemistry 234*, Springer, Heidelberg **2004**, p. 63.
[18] In the following, it will be denoted as a LMCT transition although the previous DFT analysis[11] indicates additional MLCT contributions for the complexes incorporating catecholate substituted by the more donating groups.
[19] a) W. O. Koch, H.-J. Krüger, *Angew. Chem.* **1996**, *108*, 484; *Angew. Chem. Int. Ed. Engl.* **1995**, *34*, 2671; b) M. Duda, M. Pascaly, B. Krebs, *Chem. Commun.* **1997**, 835; c) Y. Hitomi, M. Yoshida, M. Higuchi, H. Minami, T. Tanaka, T. Funabiki, *J. Inorg. Biochem.* **2005**, *99*, 755.
[20] E. Buhks, G. Navon, M. Bixon, J. Jortner, *J. Am. Chem. Soc.* **1980**, *102*, 2918.
[21] a) H. Oshio, K. Toriumi, Y. Maeda, Y. Takashima, *Inorg. Chem.* **1991**, *30*, 4252; b) Y. Maeda, H. Oshio, K. Toriumi, Y. Takashima, *J. Chem. Soc., Dalton Trans.* **1991**, 1227; c) Y. Nishida, K. Kino, S. Kida, *J. Chem. Soc,. Dalton Trans.* **1987**, 1957; d) Y. Maeda, H. Oshio, Y. Tanigawa, T. Oniki, Y. Takashima, *Bull. Chem. Soc. Jpn.* **1991**, *64*, 1522.
[22] M. Milos, C. Enachescu, A. Hauser, unpublished results.
[23] a) E. König, *Prog. Inorg. Chem.* **1987**, *35*, 527; b) P. Guionneau, M. Marchivie, G. Bravic, J.-F. Létard, D. Chasseau in *Spin Crossover in Transition Metal Compounds, Vol. II, Topics in Current Chemistry 234*, Springer, Heidelberg, **2004** p. 97; c) J. A. Real, A. B. Gaspar, V. Niel, M. C. Muñoz, *Coord. Chem. Rev.* **2003**, *236*, 121.
[24] a) F. Renz, H. Oshio, H. Spiering, V. Ksenofotnov, M. Waldeck, H. Spiering, P. Gütlich, *Angew. Chem.* **2000**, *112*, 3832; *Angew. Chem. Int. Ed.* **2000**, *39*, 3699; b) H. Oshio, H. Spiering, V. Ksenofotnov, F. Renz, P. Gütlich, *Inorg. Chem.* **2001**, *40*, 1143.
[25] A. Hauser, C. Enachescu, A. Vargas, M. Lawson, N. Amstutz, unpublished results.

Received: December 7, 2005
Revised: February 13, 2006
Published online on April 3, 2006

